San Jose State University

SJSU ScholarWorks

Faculty Publications, Biomedical, Chemical, and Materials Engineering

Biomedical, Chemical and Materials Engineering

1-1-2005

The Grain Size and Microstructure of Jet-Electroplated Damascene Copper Films

Stacy H. Gleixner
San Jose State University, stacy.gleixner@sjsu.edu

Andrew Tzanavaras
San Jose State University

Gregory Young
San Jose State University

Follow this and additional works at: https://scholarworks.sjsu.edu/chem_mat_eng_pub

Part of the Other Chemical Engineering Commons, and the Other Materials Science and Engineering Commons

Recommended Citation

Stacy H. Gleixner, Andrew Tzanavaras, and Gregory Young. "The Grain Size and Microstructure of Jet-Electroplated Damascene Copper Films" *Journal of the Electrochemical Society* (2005): c101-c107. https://doi.org/10.1149/1.1846712

This Article is brought to you for free and open access by the Biomedical, Chemical and Materials Engineering at SJSU ScholarWorks. It has been accepted for inclusion in Faculty Publications, Biomedical, Chemical, and Materials Engineering by an authorized administrator of SJSU ScholarWorks. For more information, please contact scholarworks@sjsu.edu.

Journal of The Electrochemical Society, **152** (2) C101-C107 (2005) C101
0013-4651/2005/152(2)/C101/7/$7.00 © The Electrochemical Society, Inc.

The Grain Size and Microstructure of Jet-Electroplated Damascene Copper Films

Andrew Tzanavaras, Gregory Young,[z] and Stacy Gleixner

Department of Chemical and Materials Engineering, San Jose State University, San Jose, California 95192

Electroplated damascene copper is rapidly replacing aluminum-copper alloys for on-chip interconnect metallization in advanced ultralarge scale integrated (ULSI) semiconductor devices. In addition to a high degree of (111) crystallographic texture, large defect-free grains are desired to enhance the performance and reliability of copper interconnects in such devices. The brightening additive level and dc current density of electroplating baths are two parameters that affect the process gap-filling capability and the degree of additive incorporation in these copper films. Additive incorporation can inhibit grain growth during the room-temperature recrystallization process and therefore affect the final grain size in electroplated copper films. This investigation explores the grain size and microstructure of dc jet-electroplated damascene copper films deposited as a function of current density and brightening additive level after first receiving a high-temperature annealing treatment. In 1.3 μm thick blanket films it was found that large, lognormally distributed, low-resistivity, highly twinned grains with an average diameter of 1.7-1.9 μm could consistently be produced over a wide variety of electroplating conditions. These results suggest that any grain growth inhibition factors, such as remnant electroplating impurities incorporated in the blanket film microstructure after the self-annealing process, can be effectively removed from these films with a sufficient thermal budget to create a stable grain size and microstructure.
© 2005 The Electrochemical Society. [DOI: 10.1149/1.1846712] All rights reserved.

Manuscript submitted March 15, 2004; revised manuscript received June 29, 2004. Available electronically January 13, 2005.

Copper is rapidly replacing aluminum as an interconnect metallization in ultralarge-scale integrated circuits (ULSIs) for better performance and reliability. The methods of depositing copper include physical vapor deposition (PVD), chemical vapor deposition (CVD), and electroless and electrochemical deposition (ECD) plating techniques.

Additive-enhanced ECD has received the most attention as the method for filling interconnect structures due to its high deposition rate, low cost of tool ownership, the ability to fill deep submicrometer damascene features, and the low resistivity of the plated copper. Jet electrochemical deposition (JECD) is a plating technique that utilizes rapid cathode rotation in conjunction with the impingement of jets of solution to sustain higher current densities and better gap-filling performance than those achieved with conventional ECD methods.[11]

A successful copper electroplating process for semiconductor on-chip interconnects using a damascene materials system must consistently produce defect-free, large-grained films with a high degree of (111) fiber crystallographic texture. Electroplated damascene copper films are typically deposited in the presence of organic brightening additives that are used in conjunction with other organic and inorganic additives to promote the "bottom up" filling of fine interconnect features.[1]

Such films show a tendency to recrystallize at room temperature. The semiconductor industry has coined the term "self-annealing" to describe this process.[2] The period required for the self-annealing process to occur ranges from hours to weeks, depending on process-dependent variables such as electroplating current density and brightener concentration, as well as the film thickness and level of geometrical constraint.[3-5] Postdeposition annealing treatments are added to speed the recrystallization process.[5-10]

The primary purpose of this investigation is to quantitatively evaluate the final in-plane Cu grain size and distribution in blanket, unpatterned JECD copper films after an extensive high-temperature annealing treatment using a wide range of JECD electroplating conditions that vary both the dc current density and brightening additive level.

Experimental

The Cu films used in this investigation were fabricated within the framework of a 3^2 full-factorial experimental design matrix that simultaneously varied both the brightener level and current density. Details of each of the nine experimental conditions are found in Table I. In each case, 1.3 μm JECD Cu films were deposited onto two duplicate 200 mm, Si(100) wafers with an etched 0.8 μm plasma-enhanced tetraethylosilicate (PETEOS) SiO_2 layer, a 25-30 nm CVD Ta barrier layer, and a 125 nm composite CVD-PVD Cu seed layer. The wafer samples contain 69 identical dice that are patterned with via and trenched regions of varying geometries as well as a surrounding blanket Cu film region.

DC electroplating of the Cu films was performed with a Jets Technology Jet Electroplating System using acid copper sulfate chemistry. This system is designed with a stationary cathode (wafer) and a rotating anode jet assembly (RAJA), which are in close proximity and oriented coaxially. A detailed description of the cell may be found in U.S. patent 5,421,987.[11] The deposition parameters common to all nine experimental conditions are given in Table II. The composition of the acid copper sulfate bath included Shipley-Ronal Copper Gleam PPR carrier,[12] Shipley-Ronal Copper gleam PPR additive (brightener),[12] and Enthone-OMI premixed CUBATH M acid copper electrolyte.[13] The PPR carrier is a polyalkylene glycol based solution with glycol concentration ranging between 1.0 and 10.0%. The PPR additive is a proprietary formulation containing sulfur functional groups in the sulfonate/sulfonic acid family. The measured pH of the Enthone-OMI premixed CUBATH M acid copper electrolyte was determined to be approximately 0.5. The composition of the Enthone-OMI premixed CUBATH M acid copper electrolyte is given in Table III.

The current density corresponding to each experimental condition was determined by dividing the wafer surface area by the applied dc current to the anode. The brightener level was determined from its chemical activity in the acid copper sulfate bath by con-

Table I. A summary table outlining the experimental matrix for this investigation. There are two electroplating variables, each at three levels, making this a 3^2 full-factorial design experiment.

Condition	Current density (mA/cm^2)	Additive level (mL/L)
1	15 (low)	0.75 (low)
2	45 (medium)	0.75 (low)
3	105 (high)	0.75 (low)
4	15 (low)	1.50 (medium)
5	45 (medium)	1.50 (medium)
6	105 (high)	1.50 (medium)
7	15 (low)	2.25 (high)
8	45 (medium)	2.25 (high)
9	105 (high)	2.25 (high)

[z] E-mail: glyoung@email.sjsu.edu

Downloaded on 2012-09-27 to IP 130.65.109.204 address. Redistribution subject to ECS license or copyright; see www.esltbd.org

Table III. The Enthone-OMI premixed CUBATH M acid copper sulfate electrolyte components as specified by the manufacturer.[13]

Component	Nominal value	Operating range
Copper sulfate	170 g/L	150-225 g/L
Sulfuric acid	67 g/L	59-75 g/L
Chloride ion (from HCl)	70 mg/L	50-90 mg/L

structing a calibration curve based on the cyclic voltammetric stripping (CVS) technique. The range of absolute concentrations used to construct the calibration curve was 0.0-2.50 mL/L in increments of 0.50 mL/L, requiring a total of six data points. For each analysis a constant scan rate of 100 mV/s was used between switching potentials of −2.3 and 1.5 V. The anodic peak areas from the CVS scans were calculated in units of millicoulombs (mC), and the results are summarized in Fig. 1. The results indicate a linear relationship ($R^2 = 0.993$) between the anodic peak area and the absolute brightener concentration and illustrate the accelerating effect that brighteners have on the Cu deposition rate for this bath chemistry. Bratin has also reported similar results.[14]

Using the regression equation in Fig. 1, the peak areas corresponding to each of the three brightener concentrations of interest in this study were calculated based on interpolation and the results summarized in Table IV. This information was used to maintain the proper brightening additive level in the acid copper sulfate electroplating bath while executing the experimental matrix previously shown in Table I. In Table IV an arbitrary chemical activity number, A_B, is also shown, which was obtained by normalizing these interpolated anodic peak areas to the area measured from the CVS scan for the brightener-free bath condition.

Upon completion of the experimental deposition matrix, all samples were isothermally annealed in a quartz tube chamber at 400°C for 30 min in a forming gas composed of 4% H_2/96% N_2 controlled diffusion forming gas environment. Sheet resistance measurements were then performed in the blanket film regions of each wafer sample using a KLA-Tencor Omnimap NC110 noncontact metals monitoring system, which uses Eddy Current probe technology (KLA-Tencor Corp., San Jose, CA).

To analyze the grain size and microstructure of the Cu films, an FEI 820 Dual-beam focused ion beam (FIB) SEM system was employed (FEI Company, Hillsboro, OR). In this investigation both plan-view and cross-sectional FIB images were acquired for the grain sizing and microstructural characterization of the annealed, electroplated copper samples in the unpatterned regions of the sample wafers. For each experimental condition five plan-view FIB images in the blanket Cu film regions of select dice were obtained for each of the nine experimental conditions at 5000 × magnification. For these images an ion beam voltage of 30 kV and beam current of 150 pA were employed, and the sample was tilted 52° relative to the horizontal to make the ion beam normal to the substrate surface. The region to be imaged was lightly milled using a beam current of 1000 pA to remove any surface oxide or other contamination prior to imaging.

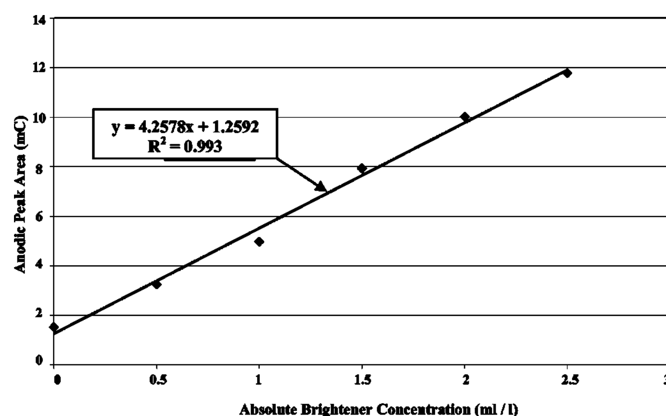

Figure 1. Derived CVS calibration curve based on the anodic peak areas calculated from the cyclic voltammograms.

For further characterization of the Cu grain structure and morphology in the blanket film regions and to determine the Cu film thickness, 2-4 tilt-view images were also acquired that allowed the microstructure to be seen in cross section. A beam voltage of 30 kV and beam current of 5 pA were typically used with magnifications ranging between 25,000 and 50,000 ×. Before such images could be acquired, a rectangular region of the Cu film was first milled down to the Si wafer using a beam current of 2700 pA. The sample was then tilted back to the horizontal position in order to make the ion beam impinge on the sidewall of the blanket film region. In this orientation, the beam was oriented 38° from the wafer surface. This leads to a foreshadowing effect that requires the Y-axis dimension of the image to be corrected before the plated Cu film thickness could be determined from the images. After a brief coarse (2700 pA) milling of the sidewall, the beam current was reduced to 1000 pA to smooth the same surface (fine milling) before imaging at 5 pA, which is below the sputtering threshold for copper.[15]

Results and Discussion

The mean sheet resistance values for all nine electroplating conditions given in Table V were found to fall within 1.7% of the mean value of 0.01265 Ω/□. A statistical analysis of the data was performed using the one-way analysis of variance (ANOVA) approach to determine if any statistically significant differences exist between experimental conditions. A derived p-value of 0.173 from the ANOVA analysis indicated there is no statistically significant difference in the mean sheet resistance between all nine experimental conditions at the 95% confidence level.

Thickness values in blanket regions of each die were determined from the tilt-view FIB images, which show the film in cross section. A total of six thickness measurements were taken from two different FIB images for each condition. The Cu film resistivities were then calculated based on the sheet resistance and thickness values for

Table II. The electrochemical deposition parameters common to all nine conditions of the experimental matrix.

Parameter	Value
Jet nozzle pressure	40 psi
Plating solution flow rate	3.5-3.8 gpm
RAJA rotation speed	20 rpm
Anode-cathode spacing	2.8 cm
Anode-cathode area ratio	0.75: 1
Collimator screen position	Not used
Wafer bias current	Not used
Deposition temperature	21.5 ± 1.0°C

Table IV. A summary of interpolated CVS peak areas for future use in monitoring and maintaining the proper brightening additive levels during subsequent electrodeposition work. An arbitrary activity number, based on the normalized peak area ratios, was also assigned to each of these three additive levels.

Brightener concentration (mL/L)	CVS peak area (mC)	A_B
0.75	4.45	2.78
1.50	7.65	4.94
2.25	10.84	7.10

Downloaded on 2012-09-27 to IP 130.65.109.204 address. Redistribution subject to ECS license or copyright; see www.esltbd.org

Table V. A summary of the measured sheet resistance and film thickness values for each experimental condition. Also shown are the calculated blanket Cu film resistivity values for each corresponding condition.

Experimental condition	R_s (Ω/□)	Thickness (μm)	Resistivity (μΩ cm)
1	0.01267	1.34	1.70
2	0.01276	1.29	1.65
3	0.01291	1.30	1.68
4	0.01220	1.35	1.65
5	0.01252	1.32	1.65
6	0.01266	1.30	1.65
7	0.01291	1.26	1.63
8	0.01259	1.28	1.61
9	0.01266	1.29	1.63
Average	0.01265	1.30	1.65
Maximum	0.01291	1.35	1.70
Minimum	0.01220	1.26	1.61
Standard deviation	0.00022	0.03	0.03
Standard deviation (%)	1.7	2.2	1.6

each die, and the results summarized in Table V. The results indicate that the films produced in this investigation approach the bulk resistivity value for Cu of 1.673 μΩ cm, for all nine conditions have similar crystalline defect densities, but not necessarily the same average grain size. Theoretical and experimental studies have shown that the grain boundary scattering contribution to the resistivity remains small and constant after the mean grain size exceeds approximately 1 μm.[2]

Typical plan-view FIB images obtained for this investigation, which use gallium ion channeling contrast, are shown in Fig. 2. From the images, one can discern large, distinct copper grains, which are indicative of complete recrystallization and subsequent grain growth of the Cu microstructure. In some cases a high degree of faceting was observed in the larger grains, which previously has been reported in the literature after high-temperature annealing treatments of electroplated copper.[7] The recrystallized microstructure also exhibits a very high degree of crystallographic twinning. Face-centered cubic (fcc) metals, such as copper and aluminum, frequently exhibit this type of defect, which comes about from stacking fault errors of the (111) close-packed planes. This type of crystalline defect can arise from either mechanical deformation or annealing.[16] In the latter case, they are generally referred to as recrystallization or annealing twins. In some cases the twinned grains exhibited very high twin densities, examples of which are illustrated in Fig. 3.

Figure 4 illustrates two cases where adjacent grains both contain twins. In the first case, the angle at the intersection of the twin boundaries is 60°, while in the second case they form an angle of 90°. Previous studies have shown that grains having a (111) crystallographic orientation have the twin boundaries that form an angle of 60°, while (200)-oriented grains have twin boundaries that intersect at an angle of 90°.[7] Both types of grains were found for all nine experimental conditions, which suggests that both (111) and (200) crystallographic texture components are present in the annealed copper films prepared for this investigation. The 60° twin boundaries, however, were observed to occur more frequently than the 90° boundaries, which raises the possibility of a larger (111) texture component.

Representative FIB images that depict the copper grain structure in cross section may be found in Fig. 5. From these images one can easily discern that the microstructure is comprised of large columnar grains that are generally of a height comparable to that of the film thickness. Similarly, the twins contained within such grains span the entire film thickness. These types of grains are most common in compact thin films and often come about as a result of preferred growth in certain crystallographic directions.[16] This is not surprising because damascene copper frequently exhibits both (111) and (200)

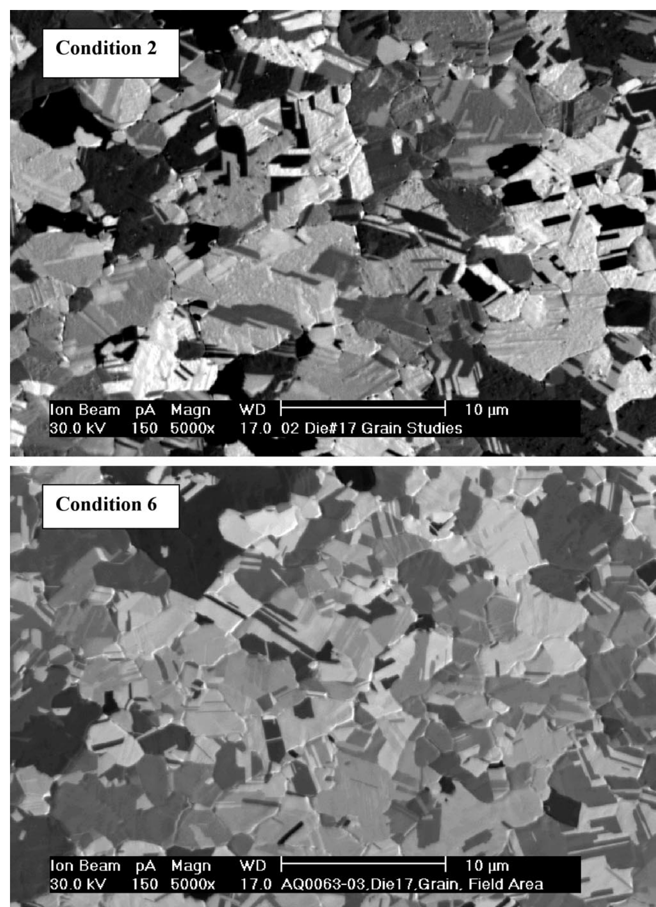

Figure 2. Representative plan-view FIB images of the annealed copper microstructure for experimental conditions (top) 2 and (bottom) 6.

texture components. Randomly oriented grains are generally small in comparison to the film thickness.[16]

The upper electron image shown in Fig. 6 shows evidence of thermal grooving where the grain boundaries intersect with the top surface of the film. The occurrence of thermal grooving is generally associated with high-temperature annealing and is a direct result of surface tension factors.[17] Diffusion of atoms over the free surfaces is believed to be the most important factor involved in the transport of atoms out of the grooved regions during the formation of the grooves. Brongersma also reported extensive grain boundary grooving in electroplated Cu films annealed at 400°C for extended periods of time.[18] However, he attributed this grooving to the grain boundary volume reduction that accompanies extensive grain growth at elevated temperatures, which generally leads to high residual tensile stresses in the films.

Lastly, circular pores, or voids, that are approximately 0.1-0.3 μm diam were also frequently observed, as is shown in the bottom tilt-view electron image of Fig. 6. Additional visual evidence of these voids was also present in plan-view FIB images and suggests they occur primarily in the grain boundaries. The origin of this undesirable film defect is unknown at this time. However, void formation has been associated with conditions of high tensile stress in soft metals that exceed the yield point.[17] In such cases, material is selectively transported out of certain regions of the film to relax the stress elsewhere. High residual tensile stresses have been shown to develop in recrystallized, electroplated Cu films during the self-annealing process for some plating chemistries,[19] or after high-temperature thermal cycling.[18]

The method used to analyze the grain size and associated grain size distributions utilized image analysis software[20] in conjunction

Downloaded on 2012-09-27 to IP 130.65.109.204 address. Redistribution subject to ECS license or copyright; see www.esltbd.org

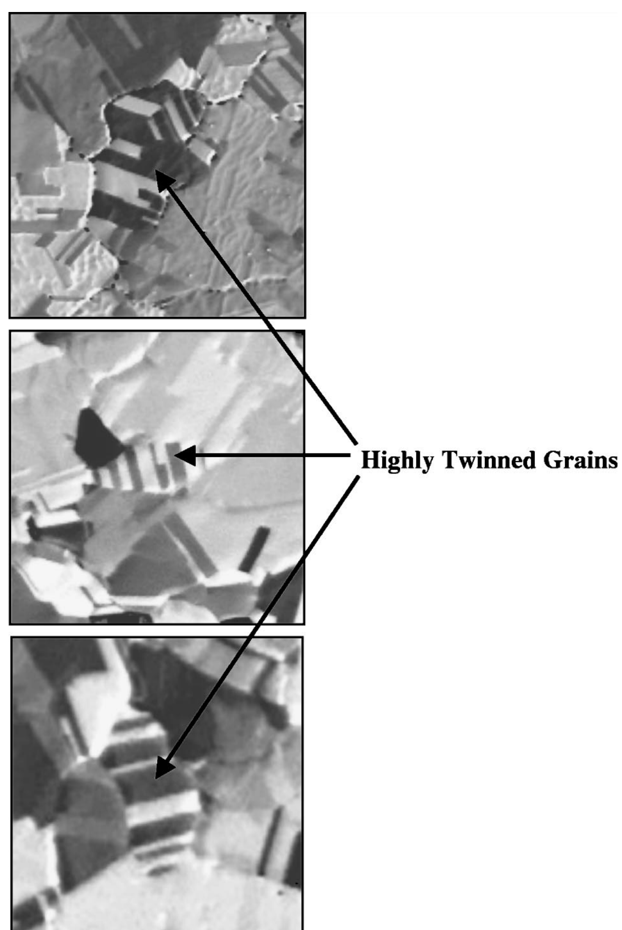

Figure 3. Examples of copper grains exhibiting a high degree of crystallographic twinning are indicted above with arrows.

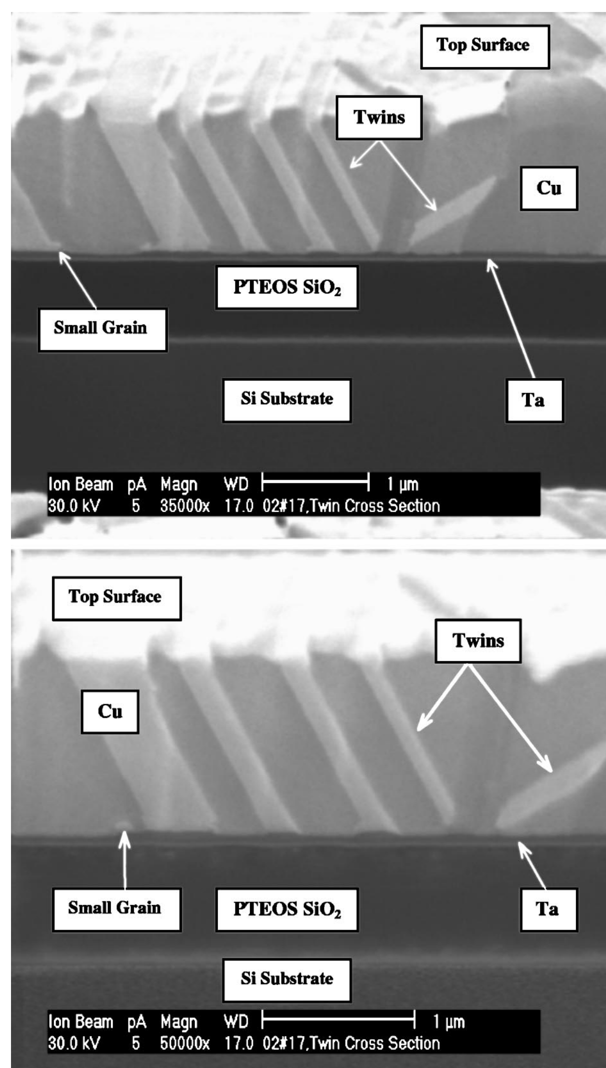

Figure 5. Tilt-view FIB images at two different magnifications showing a cross section of the annealed copper microstructure for experimental condition 6.

with plan-view FIB images taken at 5000× magnification. A total of five plan-view images in the blanket film region of select die were acquired for each of the nine experimental conditions for grain-sizing purposes. Because copper grains frequently exhibit crystallographic twins, completely automated grain sizing is not possible with FIB or even transmission electron microscopy (TEM) photomicrographs. When grain sizing polycrystalline fcc metals, it is customary not to count the twins within the copper grains separately, as they are generally considered to be subgrain boundaries. However, image analysis software packages use grayscale contrast to differentiate between grains or particles. Using automated grain detection yields some erroneous results, because a grain containing a single twin, which usually has a significantly different grayscale value, would, in effect, be treated as three separate grains. A frequently used approach to circumvent these problems is to manually trace the grain boundaries from a printed image onto an overlaid transparency and digitally scan the results into an image analysis program to calculate the individual grain areas.[21]

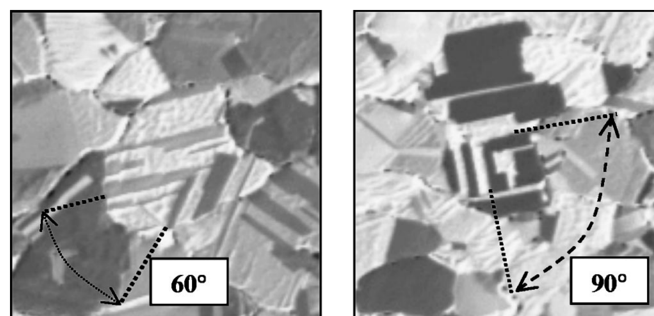

Figure 4. Examples of twin boundaries intersecting at (left) 60° and (right) 90°.

In this investigation, a combination of both manual and automated techniques were employed to determine the grain sizes and associated distributions. To perform the grain size analysis, the automatic particle detection feature of the software utility was not employed for the reasons stated above. After appropriate spatial calibration of the image to be analyzed, the grayscale thresholding feature was utilized to narrow the grayscale detection range to approximately 20-30 grayscale levels, starting with the low (dark) side of the grayscale level spectrum. Grains that were discernable to a reasonable degree of confidence within a given grayscale range were then manually traced directly on the image and numbered. Special precautions were taken to ensure accurate grain identification in cases where the grains were twinned, had very similar grayscale levels, or indistinct grain boundaries. This included utilization of image enhancement features such as zoom, contrast, brightness, and the application of various image filters contained within the software utility.

Downloaded on 2012-09-27 to IP 130.65.109.204 address. Redistribution subject to ECS license or copyright; see www.esltbd.org

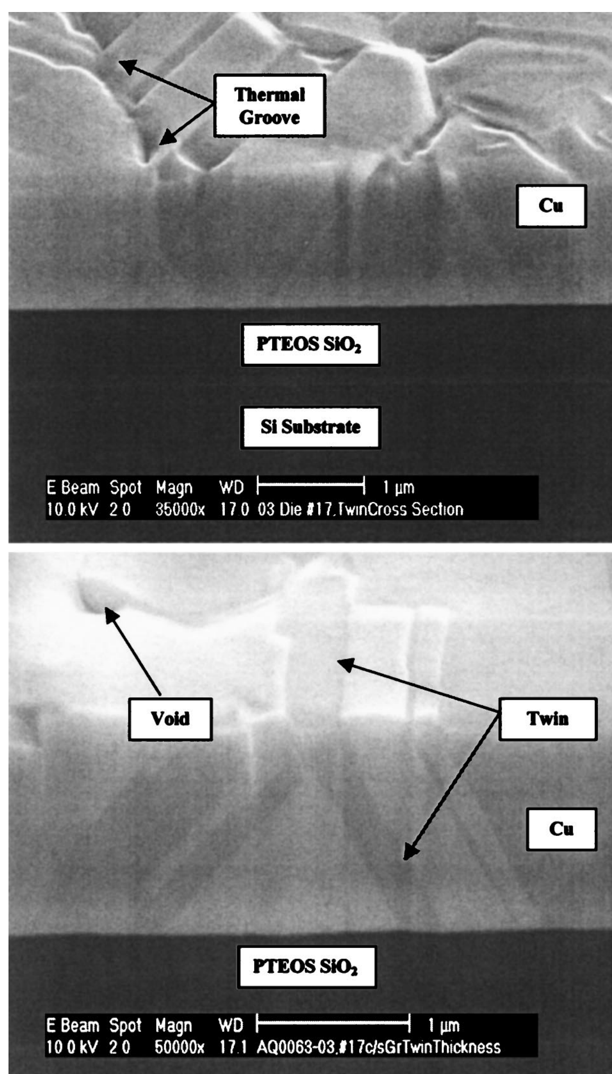

Figure 6. Two tilt-view electron images of the annealed blanket Cu films from experimental condition 2 showing (top) thermal grooving and (bottom) a void.

The areas of each numbered grain in this collection were then calculated with the area analysis feature of the software. The process was then repeated approximately ten times for each image to encompass the entire range of grayscales contained within the image. The areas of approximately 500-600 grains for each of these conditions were acquired and analyzed.

The in-plane, mean grain size and standard deviation for each condition were determined from a Gaussian fit to the distribution of grain sizes. This method assumes circular two-dimensional grains, because the data were generated from areal FIB images. In essence, this method assumes a linear correlation between two-dimensional (areal) and three-dimensional (volume) recrystallization. This method is commonly used and well documented in the literature for studies that employ FIB plan-view imaging for grain sizing.[7,22]

A graphical summary of the basic univariate grain size statistics for all nine experimental conditions is shown in Fig. 7. The mean grain diameters ranged between 1.7 and 1.9 μm, with standard deviations that ranged between 0.5 and 0.8 μm. A grain size that is large in comparison to the film thickness has been attributed to abnormal, or nonuniform, growth during the annealing process.[23] This is consistent with the contention of many authors that additive incorporation in Cu grain boundaries is a factor that contributes to

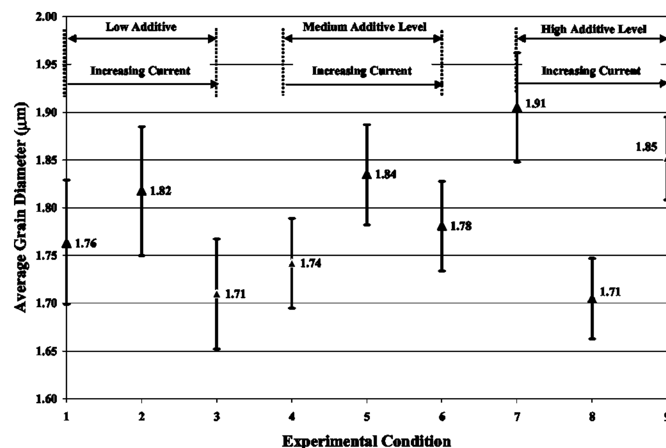

Figure 7. Plot summarizing the grain sizing results for all nine experimental conditions. Vertical error bars shown in red represent the 95% confidence intervals.

the initiation of abnormal grain growth during the recrystallization process.[2,24,25]

These results show that a high-temperature annealing treatment of blanket, self-annealed copper films produces large grains of similar dimensions that are independent of the dc current density or additive level used during the copper electrodeposition process for the range of values studied. Considering the degree of overlap of the 95% confidence intervals shown in Fig. 7 and the inherent potential for some error to be generated in the grain-sizing process, these data suggest that no statistically significant difference in the mean grain sizes exists after high-temperature annealing. These results are in agreement with and complementary to the work of Brongersma, who showed that extensive annealing at high temperatures results in an additional considerable enlargement of the grain structure accompanied by an additional decrease in the sheet resistance and the desorption of impurities that were incorporated during the electroplating process.[18]

The grain size results are also in agreement with the resistivity results, which showed no significant differences in the bulk film resistivity for any of the nine experimental conditions. Films with similar grain sizes would be expected to have similar resistivities, assuming the same film thickness and similar defect densities. However, the reader should be cautioned that the resistivity increase attributable to grain boundary scattering in Cu thin films becomes relatively insignificant ($<5\%$) once the grain size reaches approximately 1 μm.[2]

The grain structure of polycrystalline thin films of fcc metals such as copper is well represented by a lognormal distribution.[23] A representative histogram of grain sizes for experimental condition 5 is shown in Fig. 8. The high degree of positive skewness and kurtosis seen in the shape of the distribution are typical of lognormal distributions. The probability density function (PDF) of a two-parameter lognormal distribution is given by

$$f(x) = \frac{1}{xb\sqrt{2\pi}} e^{-(1/2b^2)[\ln(x)-a]^2} \qquad [1]$$

where $f(x)$ is the probability density function, x is the grain size, and a and b are parameters that define the shape of the distribution.[26] The mean (μ) and variance (σ^2) of x are related to these shape parameters by[26]

$$\mu = e^{a+0.5b^2} \qquad [2]$$

$$\sigma^2 = \mu^2(e^{b^2} - 1) \qquad [3]$$

Downloaded on 2012-09-27 to IP 130.65.109.204 address. Redistribution subject to ECS license or copyright; see www.esltbd.org

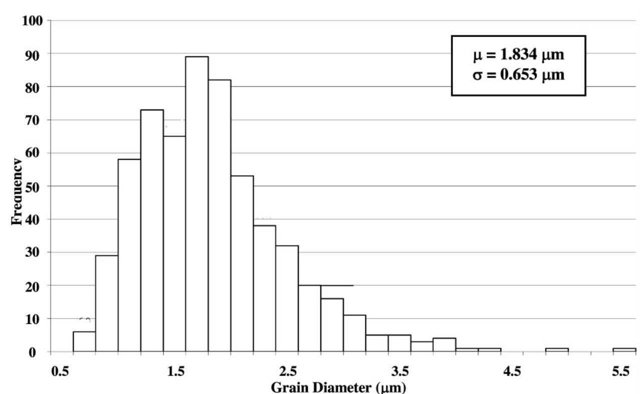

Figure 8. Representative histogram of grain sizes obtained for experimental condition 5. The shape of the distribution suggests a high degree of positive skewness and kurtosis, which is typical of lognormal distributions. The mean grain size (μ) and standard deviation (σ) are also shown.

The simplest way to fit the distribution to a set of grain size data is to take the natural logarithms and set a and b equal to the mean and standard deviations of these transformed data. The data shown in Fig. 8 yielded values of 0.547 and 0.345 for the lognormal shape parameters a and b, respectively. The resulting probability density function for the data of condition 5 is shown in Fig. 9. The values of a and b for all nine conditions, along with the associated means and variances derived from Eq. 2 and 3, are summarized in Table VI.

In accordance with the Central Limit Theorem, this results in a set of data that is normally distributed.[26] A simple test for any serious deviations from lognormality would then be to first logarithmically transform the data and then construct a normal probability plot of the resulting data. If the data is normally distributed, the points on a normal probability plot should fall close to a straight line. A normal probability plot for the data of condition 5 is shown in Fig. 10. This figure shows that the data are normally distributed ($R^2 = 0.998$) and only minor deviations from normality exist at the extreme ends of the data set. It can thus be inferred that the data for condition 5 are lognormally distributed and are an excellent fit to a lognormal distribution of grain sizes. Similar results were obtained for the remaining eight experimental conditions.

Based on the previous discussion, it is evident that the grain size distributions of blanket electroplated copper films remain lognormal in character after a high-temperature annealing process. These results are consistent with a study by Beyer that reported a lognormal distribution of grain sizes for a 1.3 μm electroplated copper film that

Table VI. The distribution parameters derived for the lognormal probability density function and associated mean and variance values for all nine experimental conditions. The results suggest very similar grain size distributions.

Condition	a	b	μ (μm)	^{2} (μm^2)
1	0.476	0.430	1.766	1.380
2	0.501	0.436	1.815	1.465
3	0.444	0.400	1.689	1.231
4	0.501	0.332	1.744	1.249
5	0.547	0.345	1.834	1.394
6	0.528	0.310	1.779	1.282
7	0.580	0.363	1.908	1.527
8	0.487	0.305	1.705	1.174
9	0.575	0.285	1.851	1.367

was annealed at 400°C using a rapid thermal processing (RTP) treatment immediately after electrodeposition.[7] A lognormal distribution of grain sizes is generally associated with abnormal or secondary grain growth, where certain thermodynamically favored grains grow at the expense of others. The results of this study, RTP studies,[7] and self-annealing studies[8] suggest that the recrystallization and subsequent grain growth of electroplated copper films proceed by an abnormal grain growth mechanism. Any fine grains remaining in the matrix after room-temperature recrystallization will grow and coalesce, or be consumed by the growth of larger recrystallized grains after a high-temperature annealing treatment. Concurrent with these processes would be the removal of any remaining crystalline defects and the desorption of any remnant solute impurities trapped at the grain boundaries that would impede further grain growth after room-temperature recrystallization is complete.

Conclusions

The results of this study have shown that a large-grained microstructure can be achieved in unpatterned damascene copper thin films for a wide variety of dc jet electroplating conditions when a high-temperature treatment follows the self-annealing process. In all cases the blanket copper films exhibited equivalent sheet resistance values at the 95% confidence level and resistivities that approach the bulk value of 1.67 μΩ cm for copper. For all nine experimental conditions, the blanket film microstructure consisted of large columnar grains that spanned the entire film thickness of 1.3 μm and exhibited a high degree of crystallographic twinning. The consequences of the thermal grooving and pores observed in the grain boundaries, which may have resulted from the high-temperature annealing treatment, are unclear at this time and require further inves-

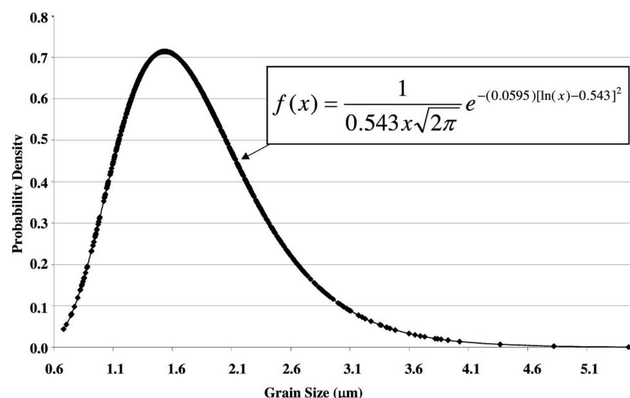

Figure 9. Lognormal probability density function for the distribution of grain sizes from experimental condition 5. Areas under the curve correspond to probabilities.

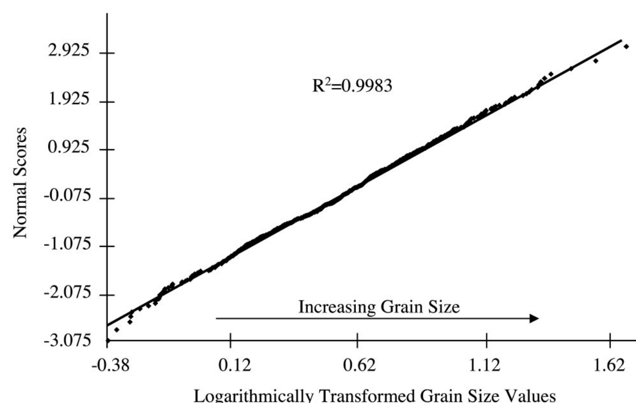

Figure 10. Normal probability plot of the logarithmically transformed grain size data from condition 5. The high degree of linearity indicates that the transformed data is normally distributed and therefore indicates a good fit to a lognormal distribution.

Downloaded on 2012-09-27 to IP 130.65.109.204 address. Redistribution subject to ECS license or copyright; see www.esltbd.org

tigation. The angles observed between grain boundaries in these Cu films suggest a large (111) crystallographic component and a lesser (200) component.

The average, in-plane grain diameters in these blanket copper films ranged between 1.7 and 1.9 μm, with large standard deviations ranging from 0.5 to 0.8 μm. Within a current density range of 15-105 mA/cm^2 and brightener level range of 0.75-2.25 mL/L, there was no statistically significant difference in the mean grain size at the 95% confidence level after the post-self-annealing, high-temperature treatment. These results suggest that any grain growth inhibition factors, such as remnant electroplating impurities incorporated in the blanket film microstructure after the self-annealing process, can be effectively desorbed from these films with a sufficient thermal budget.

For all nine conditions the grain-size distributions were found to have similar lognormal characteristics, which suggests abnormal grain growth during both the recrystallization and subsequent grain growth processes. The largest grain sizes in these distributions were found to be four to five times the blanket film thickness, which is characteristic of abnormal grain growth. Future work will explore the crystallographic texture of these same blanket films by X-ray diffraction and the microstructure and grain size within the fine damascene trench features on the experimental wafers used in this study.

San Jose State University assisted in meeting the publication costs of this article.

References

1. R. D. Mikkola, Q. T. Jiang, R. Carpio, and B. Carpenter, *Mater. Res. Soc. Symp. Proc.,* **564**, 399 (1999).
2. J. M. E. Harper, C. Cabral, P. C. Andricacos, L. Gignac, I. C. Noyan, K. P. Rodbell, and C. K. Hu, *Mater. Res. Soc. Symp. Proc.,* **564**, 387 (1999).
3. T. Ritzdorf, D. Chen, D. Fulton, and C. Dundas, in *IEEE IITC Conference Proceedings*, p. 287 (1999).
4. S. H. Brongersma, E. Richard, I. Vervoot, and K. Maex, in *IEEE IITC Conference Proceedings*, p. 31 (2000).
5. Q. T. Jiang, M. E. Thomas, G. Bersuker, B. Foran, R. Mikkola, C. Carpenter, and J. Ormando, *Mater. Res. Soc. Symp. Proc.,* **564**, 429 (1999).
6. M. Chen, H. S. Shin, R. Cheung, R. Morad, Y. Dordi, S. Rengarajan, and S. Tsai, in *IEEE IITC Conference Proceedings*, p. 194 (2000).
7. G. P. Beyer, P. Kitabijan, S. H. Brongersma, H. Bender, E. Richard, I. Vervoort, P. Hey, P. Zhang, and K. Maex, in *Materials Research Society Advanced Metallization Conference Proceedings (AMC 99)*, Sept 1999, p. 75 (1999).
8. V. M. Dubin, G. Morales, C. Ryu, and S. S. Wong, *Mater. Res. Soc. Symp. Proc.,* **505**, 137 (1998).
9. V. M. Dubin, C. H. Ting, and R. Cheung, in *ISMIC VMIC Conference Proceedings*, June 1997, p. 69 (1997).
10. V. M. Dubin, S. Lopatin, S. Chen, R. Cheung, C. Ryu, and S. S. Wong, *Mater. Res. Soc. Symp. Proc.,* **514**, 275 (1998).
11. G. Tzanavaras and U. Cohen, U.S. Pat. 5,421,987 (1995).
12. LeaRonal Tech Spec, Copper Gleam PPR, Product Code TS-30013, Shipley Ronal, Marlborough, MA, 0.752 (1998).
13. Sel-Rex CUBATH M, Technical Data Sheet, Product Code DCJ0, Enthone-OMI, Inc., New Haven, CT 03235 (1998).
14. P. Bratin, G. Chalyt, and M. Pavlov, in *Proceedings of the AESF Annual Technical Conference*, p. 149 (1999).
15. T. K. Olson, R. G. Lee, and J. C. Morgan, in *Proceedings 18th International Symposium for Testing and Failure Analysis (ISTFA 92)*, p. 373 (1992).
16. M. Paunovic and M. Schlesinger, *Fundamentals of Electrochemical Deposition*, pp. 169, 247-243, John Wiley & Sons, Inc., New York (1998).
17. R. E. Reed-Hill and R. Abbaschian, *Physical Metallurgy Principles, International Student Edition*, pp. 227-269, 264-266, 549-550, 741-742, PWS-Kent Publishing Company, Boston, MA (1992).
18. S. H. Brongersma, E. Richard, I. Vervoot, K. Maex, E. Kerr, and A. Saerens, *J. Mater. Res.,* **17**, 582 (2002).
19. R. D. Mikkola, Q. T. Jiang, and B. Carpenter, *Plat. Surf. Finish.,* **87**(3), 81 (2000).
20. D. Wilcox, B. Dove, D. McDavid, and D. Greer, UTHSCSA Image Tool for Windows (Version 2.00), University of Texas Health Science Center, San Antonio, TX (1995-1996).
21. P. Justison, E. Ogawa, M. Gall, C. Capasso, D. Jawarani, J. Wetzel, and P. S. Kawasaki, in *IEEE IITC Conference Proceedings*, p. 202 (2000).
22. L. M. Gignac, K. P. Rodbell, C. Cabral, Jr., P. C. Andricacos, P. M. Rice, R. B. Beyers, P. S. Locke, and S. J. Klepeis, *Mater. Res. Soc. Symp. Proc.,* **564**, 373 (1999).
23. D. P. Tracy and D. B. Knorr, *J. Appl. Phys.,* **76**, 2671 (1994).
24. S. P. Hau-Riege and C. V. Thompson, *Appl. Phys. Lett.,* **6**, 309 (2000).
25. J. M. E. Harper, C. Cabral, P. C. Andricacos, L. Gignac, I. C. Noyan, K. P. Rodbell, and C. K. Hu, *J. Appl. Phys.,* **86**, 2516 (1999).
26. A. V. Metcalfe, *Statistics in Engineering, A Practical Approach*, Texts in Statistical Science, pp. 97-99, Chapman and Hall, New York (1994).

Downloaded on 2012-09-27 to IP 130.65.109.204 address. Redistribution subject to ECS license or copyright; see www.esltbd.org